Universiteit
Leiden
The Netherlands

Surface formation routes of interstellar molecules : a laboratory study

Sergio, I.

Citation
Sergio, I. (2010, December 9). *Surface formation routes of interstellar molecules : a laboratory study*. Retrieved from https://hdl.handle.net/1887/16228

Version:	Corrected Publisher's Version
License:	Licence agreement concerning inclusion of doctoral thesis in the Institutional Repository of the University of Leiden
Downloaded from:	https://hdl.handle.net/1887/16228

Note: To cite this publication please use the final published version (if applicable).

CHAPTER 4

Water formation at low temperatures by surface O_2 hydrogenation I: characterization of ice penetration[1]

Water is the main component of interstellar ice mantles, is abundant in the solar system and is a crucial ingredient for life. The formation of this molecule in the interstellar medium cannot be explained by gas phase chemistry only and its surface hydrogenation formation routes at low temperatures (O, O_2, O_3 channels) are still unclear and most likely incomplete. In Chapter 3 we discussed an unexpected zeroth-order H_2O production behavior in O_2 ice hydrogenation experiments compared to the first-order H_2CO and CH_3OH production behavior found in former studies on hydrogenation of CO ice. In this chapter we experimentally investigate in detail how the structure of O_2 ice leads to this rare behavior in reaction order and production yield. In our experiments H atoms are added to a thick O_2 ice under fully controlled conditions, while the changes are followed by means of Reflection Absorption InfraRed Spectroscopy (RAIRS). The H-atom penetration mechanism is systematically studied by varying the temperature, thickness and structure of the O_2 ice. We conclude that the competition between reaction and diffusion of the H atoms into the O_2 ice explains the unexpected H_2O and H_2O_2 formation behavior. In addition, we show that the proposed O_2 hydrogenation scheme is incomplete, suggesting that additional surface reactions should be considered. Indeed, the detection of newly formed O_3 in the ice upon H-atom exposure proves that the O_2 channel is not an isolated route. Furthermore, the addition of H_2 molecules is found not to have a measurable effect on the O_2 reaction channel.

[1]Based on: S. Ioppolo, H. M. Cuppen, C. Romanzin, E. F. van Dishoeck, H. Linnartz, 2010, Physical Chemistry Chemical Physics, volume 12, pages 12065-12076

4.1 Introduction

The presence of water is a prerequisite for the origin of life as we know it and, even though the ubiquity and abundance of water ice in space (*i.e.*, dense molecular clouds, protoplanetary disks and solar-like systems) is well established by infrared observations (Gillett & Forrest 1973, Dartois et al. 1998, Whittet 2003, Gibb et al. 2004, Boogert et al. 2008), the chemical origin of water is not yet well understood. Among the various molecules detected in the solid phase in dense molecular clouds, water is the dominant component of interstellar icy grain mantles. In such environments, the observed abundance of water ice cannot be explained by direct accretion from the gas phase only. Indeed, theoretical models predict that grain surface reactions play an essential role in water formation (Tielens & Hagen 1982, d'Hendecourt et al. 1985, Hasegawa et al. 1992, Hasegawa & Herbst 1993, Cuppen & Herbst 2007).

Tielens & Hagen (1982) proposed a reaction scheme in which solid water ice is formed on grain surfaces by hydrogenation of atomic oxygen, molecular oxygen and ozone. Using a Monte Carlo approach, Cuppen & Herbst (2007) showed that the contribution of the different formation channels strongly depends on the local environment in interstellar clouds. They concluded that the atomic oxygen channel is the main route in translucent and diffuse clouds, while the molecular oxygen channel, together with the ozone route, is more efficient in dense cold molecular clouds. However, these theoretical results on surface reactions are largely based on gas phase input data and these data should not be extrapolated directly to the solid phase. A systematic laboratory investigation of water ice formation at interstellar relevant temperatures (~10 K) is therefore highly needed to confirm these reaction routes.

The suggested water formation channel with the smallest number of steps is the hydrogenation of O atoms:

$$H + O \rightarrow OH, \tag{4.1}$$

$$H + OH \rightarrow H_2O, \tag{4.2}$$

and

$$H_2 + OH \rightarrow H_2O + H. \tag{4.3}$$

From gas phase data, it is clear that the radical-radical reactions (4.1) and (4.2) proceed without activation barriers. Recently, Atkinson et al. (2004) reviewed reaction (4.3), assigning it a gas phase barrier of 2100 K, instead of 2600 K as assumed earlier (Schiff 1973). Preliminary investigations on the H + O (D + O) channel in the solid phase have been carried out by Hiraoka et al. (1998) and Dulieu et al. (2010). Both groups reported the formation of D_2O by temperature programmed desorption (TPD) through reactions of D and O atoms on a N_2O matrix and an annealed amorphous H_2O ice, respectively. Since the TPD technique does not allow to distinguish between water formed at low temperature and during heating, a quantitative interpretation of these results is not straight-forward.

The hydrogenation of ozone proceeds through the formation of OH and O_2:

$$H + O_3 \rightarrow OH + O_2. \tag{4.4}$$

The hydroxyl radical can be further hydrogenated via reactions (4.2) and (4.3). Mokrane et al. (2009) reported experimental evidence for water formation via ozone deuteration at 10 K using again TPD for analysis. Also here, the exclusive use of a quadrupole mass spectrometer for the analysis of the surface reaction final products led to a qualitative study. Recently, Romanzin et al. (2010) investigated water formation via ozone hydrogenation/deuteration at different temperatures, combining infrared spectroscopy with mass spectrometry as a probe for the identification of the ongoing surface processes (see Chapter 6).

The hydrogenation of molecular oxygen results in the formation of water through the following steps:

$$H + O_2 \rightarrow HO_2 \tag{4.5}$$

$$H + HO_2 \rightarrow H_2O_2 \tag{4.6}$$

$$H + H_2O_2 \rightarrow H_2O + OH. \tag{4.7}$$

This O_2 channel is the best studied solid-phase route to form water in the literature. Reactions (4.5) and (4.6) have no activation barriers Troe & Ushakov (2008), Keyser (1986) while reaction (4.7) has a gas phase activation energy of ∼1800 K (Baulch et al. 1992). Reactions (4.2) and (4.3) are also included in this channel. Several groups have explored the O_2 hydrogenation reaction route independently in the solid phase (Miyauchi et al. 2008, Ioppolo et al. 2008, Matar et al. 2008, Oba et al. 2009) and this channel is also the topic of the present chapter. The experimental procedure used here is similar to the one described in (Miyauchi et al. 2008, and Chapter 3).

In Chapter 3 we exposed 15 ML (1 ML $\sim 10^{15}$ molecules cm^{-2}) of solid O_2 to H/D atoms, covering a large range of ice temperatures from 12 K to 28 K. A comparison between the experimental results presented in Chapter 3 and obtained here, is reported in § 4.3.1 which discusses the temperature dependence. For all investigated temperatures shown in Chapter 3, we observed an initial linear and temperature independent growth of the products, H_2O_2/D_2O_2 and H_2O/D_2O, which corresponds to a zeroth-order formation rate. The final yield was found to be temperature dependent. Surface reactions are usually considered to follow second order dynamics, since they depend on the diffusion of two reactants. Because of the constant H-atom flux in the surface reaction experiments, which results in a constant abundance of one of the reactants, namely H, this will effectively lead to first order behavior. Our observation of zeroth order kinetics therefore came as a surprise. Hence, we decided to use an effective model to fit our results reflecting a zeroth order behavior. We considered two regimes to describe the initial linear temperature independent growth and the temperature dependent final yield, respectively. In the first regime, the H_2O_2/D_2O_2 is formed following a zeroth-order rate, while H_2O/D_2O follows a usual first order rate. In the second regime, both products follow first-order behavior. This method gives the correct functional form to describe the experimental results, whereas a first-order model over the entire regime does not. This is especially apparent at high temperatures. In contrast, Miyauchi et al. (2008) used a diffusive, first-order model to fit their hydrogenation/deuteration results, investigating only experiments at a low temperature of 10 K, where the zeroth-order behavior is less prominent.

Oba et al. (2009) stated that the physicochemical meaning of this model is unclear. However, in Chapter 3, we explained our two phase model by the following scenario. Initially, the incoming H atoms diffuse into the ice with an efficiency that is independent of temperature. Once an H atom is trapped in the ice, it can diffuse efficiently and find an oxygen molecule to react with. When nearly all oxygen molecules within the penetration depth, which is temperature dependent, are converted to H_2O_2/D_2O_2, diffusion becomes rate limiting. According to our model no large isotope effect was found for reaction (4.7). Using their diffusive model, Miyauchi et al. (2008) did find a significant isotope effect for this reaction. Our results, however, suggest that the reaction can proceed with a low barrier or that additional mechanisms for water formation should be taken into account in the model to fit the data.

In order to resolve this issue, we provide here the experimental verification of our scenario for a non-standard behavior, *i.e.*, for an initially linear and temperature independent growth of the reaction products with a final yield that is temperature dependent. For this purpose, the penetration mechanism of H atoms into the O_2 ice is studied experimentally and we discuss in detail the different possible origins for the temperature dependent penetration depth. Our further objective is to study several surface reaction mechanisms leading to H_2O formation under laboratory conditions for different temperatures, thicknesses and structures of the O_2 ice. In Chapter 5 we focus on unravelling the reaction scheme with an emphasis on alternative H_2O formation routes to explain the lacking isotope effect.

In the following sections we present the experimental and data analyzing methods, the results and discussion, which include temperature dependence, thickness dependence, structural effect, penetration mechanism, and H_2 dependence, and – in the last section – we summarize the main conclusions of this study.

4.2 Experimental and data analysis

4.2.1 Experimental

All experiments are performed in an ultra high vacuum setup (SURFRESIDE), which consists of a stainless steel vacuum main chamber and an atomic line. Details are available from Ioppolo et al. (2008), Fuchs et al. (2009). The room temperature base pressure of the vacuum system is in the 10^{-10} mbar regime. A schematic view of the experimental apparatus is shown in Fig. 4.1. The gold coated copper substrate (2.5×2.5 cm^2), placed in the center of the main chamber, is in thermal contact with a cold finger of a close-cycle He cryostat. The substrate temperature is controlled between 12 and 300 K with a precision of 0.5 K. The absolute temperature accuracy is better than 2 K. An all-metal leak valve is used to admit gaseous O_2 (99.999% purity, Praxair) into the chamber, where it condenses onto the substrate for temperatures below ~30 K (Acharyya et al. 2007). Deposition proceeds under an angle of 45° and with a controllable flow between 10^{-8} and 10^{-7} mbar s^{-1}, where 1.3×10^{-6} mbar s^{-1} corresponds to 1 Langmuir (L). According to the measurements presented here 1 ML corresponds to 3 L (see § 4.3.4). Diatomic

homonuclear molecules like O_2 are infrared in-active, except when embedded in an ice matrix (Ehrenfreund et al. 1992). Hence, gas phase O_2 is monitored during the deposition mass spectrometrically using a quadrupole mass spectrometer (QMS) with a Faraday cup, which is placed behind the substrate and opposite to the atomic source.

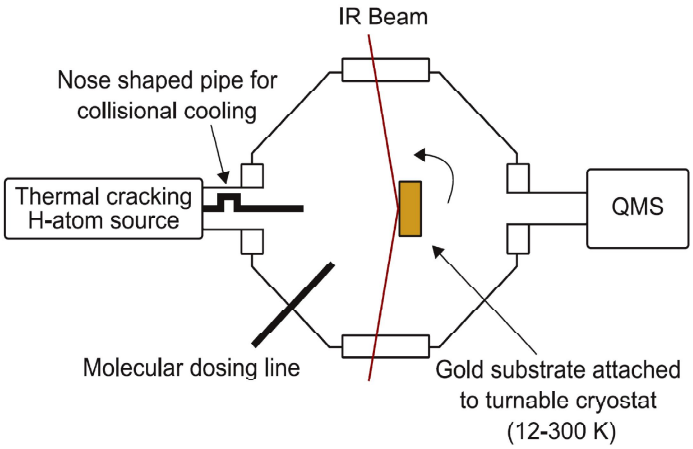

Figure 4.1 Schematic top-view of the solid-state experimental UHV set-up.

A second precision leak valve is used to admit H_2 molecules (99.8% purity, Praxair) into the capillary of a well-characterized thermal cracking source (Tschersich & von Bonin 1998, Tschersich 2000, Tschersich et al. 2008), which is used to hydrogenate our O_2 sample through heating the capillary from 300 to 2250 K by a surrounding tungsten filament. During the experiments the H + H_2 flow through the capillary and the temperature of the tungsten filament are controlled and kept constant. A quartz pipe is placed along the path of the dissociated beam. The nose-shaped form of the pipe is designed to efficiently thermalize all H atoms to room temperature through surface collisions *before* they reach the ice sample. The geometry is designed in such a way that this is realized through at least four collisions of the H-atoms with the walls before leaving the pipe. In this way, hot species (H; H_2) cannot reach the ice directly. Furthermore, previous experiments with liquid nitrogen cooled atomic beams did not show any H/D-atom temperature dependence in the O_2 hydrogenation reaction process (Miyauchi et al. 2008, Oba et al. 2009). It is important to note that the relatively high temperature of 300 K of the incident H atoms in our experiments does not affect the experimental results, since H atoms are thermally adjusted to the surface temperature as has been shown in Chapter 2.

In this work, atomic fluxes are measured at the sample position in the main chamber, following the procedure described in Hidaka et al. (2007). The H-atom flux used for all our experiments is 2.5×10^{13} atoms cm^{-2} s^{-1} for a filament temperature of 2200 K and an atomic chamber pressure of 1×10^{-6} mbar and confirms the value used within the errors in Chapter 2 and 3. The atomic beam is normal to the substrate surface except for the experiment regarding the angle dependence, which is reported in § 4.3.2. Details about

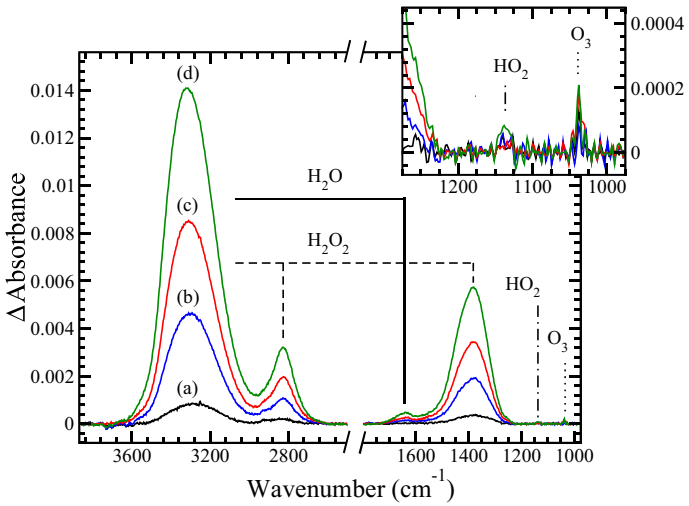

Figure 4.2 RAIR spectral changes of the O_2 ice at 25 K as a function of the H-atom fluence: (a) 4.5×10^{15}, (b) 3.7×10^{16}, (c) 7.5×10^{16}, and (d) 1.5×10^{17} atoms cm^{-2}.

the H- and D-atom flux determination are given in Appendix A.

Ices are monitored by means of RAIRS using a Fourier Transform InfraRed Spectrometer (FTIR), which covers the range between 4000 and 700 cm^{-1} (2.5−14 μm). A spectral resolution of 4 cm^{-1} is used and 512 scans are co-added. RAIR difference spectra (Δ*Absorbance*) with respect to the initial O_2 ice are acquired every few minutes during H/D exposure. Newly formed solid H_2O/D_2O and H_2O_2/D_2O_2 in hydrogenation/deuteration experiments are detected using RAIRS. Table 4.1 shows an extensive list summarizing different ice thicknesses and temperatures for which the O_2 hydrogenation is investigated. Additional experiments are performed to study the effect of ice structure, the H-atom penetration mechanism into the ice and the role of H_2 in the hydrogenation reaction scheme. Deuteration experiments are also performed for control purposes.

4.2.2 Data analysis

After fitting the infrared spectra with a straight baseline, the column densities (molecules cm^{-2}) of the newly formed species are determined from the integrated intensity of the infrared bands using a modified Lambert-Beer equation (Bennett et al. 2004):

$$N_X = \frac{\int A(\nu)\mathrm{d}\nu}{S_X} \tag{4.8}$$

where $A(\nu)$ is the integrated absorbance and S_X is the corresponding band strength. This equation can however only be used for thin layers. Teolis et al. (2007) showed that the proportionality between the optical depth and the ice abundance breaks down for thick

Table 4.1 List of experiments. The ice thickness is expressed in monolayers (ML); R_{dep} is the O_2 deposition rate; T_{dep} is the substrate temperature during O_2 deposition; $T_{H/D-add}$ is the substrate temperature during H/D-atom addition; P_{AL} is the atomic line pressure during the H/D-atom exposure; T_{AL} is the tungsten filament temperature; H/D-atom fluence is the total fluence at the end of the experiment; t is the time of the H/D-atom addition which includes, in some cases, the ramping time when changing temperature.

O_2 Thickness (ML)	R_{dep} (ML min^{-1})	T_{dep} (K)	$T_{H/D-add}$ (K)	P_{AL} (10^{-6} mbar)	T_{AL} (K)	H/D-atom fluence (10^{17} atoms cm^{-2})	t (min)
Control experiments						(H/D)	
co-deposition[a]	–	60	60	1	2200	1.3	90
25[b]	1.5	15	15	1	2200	2.7	180
35[c]	0.7	15	25	1	2200	2.7	180
25[d]	1.5	15	25	1	300	–	150
100[e]	1.5	15	28	1	2200	4.5	300
15[f]	0.7	15	25	1	2200	1.5	100
Temperature dependence						(H)	
35	0.7	15	15	1	2200	2.2	150
35	0.7	15	18	1	2200	2.2	150
35	0.7	15	20	1	2200	2.2	150
35	0.7	15	23	1	2200	2.2	150
35	0.7	15	25	1	2200	2.2	150
35	0.7	15	26	1	2200	2.7	180
35	0.7	15	27	1	2200	3.3	220
Structural effect							
25[g]	1.5	15	15	1	2200	1.8	125
25[h]	1.5	15	15	1	2200	0.22	125
35[i]	0.7	15	25	1	2200	1.9	130
Penetration mechanism							
25[j]	1.5	15	15→25	1	2200	1.6	130
25[k]	1.5	15	25→15	1	2200	2.1	160
35[l]	0.7	15	25→15	1	2200	2.5	190
Thickness dependence							
1	0.15	15	25	1	2200	2.2	150
3	0.15	15	25	1	2200	2.2	150
5	0.15	15	25	1	2200	2.2	150
8	0.15	15	25	1	2200	1.8	125
12	0.15	15	25	1	2200	2.2	150
25	0.15	15	25	1	2200	2.2	150
35	0.15	15	25	1	2200	2.2	150
70	1.5	15	25	1	2200	1.9	130
90	1.5	15	25	1	2200	3.0	200
H_2 dependence							
25	1.5	15	25	10	1850	2.2	150
25	1.5	15	25	1	2200	2.2	150
25	1.5	15	25	0.5	2250	2.2	150

[a] Simultaneous deposition of O_2 and D atoms. [b] An inert layer of $^{15}N_2$ ice is used instead of solid O_2. [c] D-atom beam. [d] H_2 added to the O_2 ice. [e] H-atom beam. [f] Thin O_2 layer deposited at 15 K on top of 100 ML of compact H_2O ice deposited at 120 K. [g] The ice is annealed at 25 K before H-atom addition. [h] H-atom addition is stopped upon saturation of the H_2O_2. [i] H-atom beam at 45° with respect to the substrate. [j] H-atom addition at 15 K is stopped after 31 minutes; the ice is heated to 25 K with 1 K min^{-1} rate; H atoms are added for 79 minutes. [k] H-atom addition at 25 K is stopped after 31 minutes; the ice is cooled to 15 K with 1 K min^{-1} rate; H atoms are added for 109 minutes. [l] H-atom addition at 25 K is stopped beyond saturation of the H_2O_2 after 100 minutes; the ice is cooled to 15 K with 1 K min^{-1} rate; H atoms are added for 70 minutes.

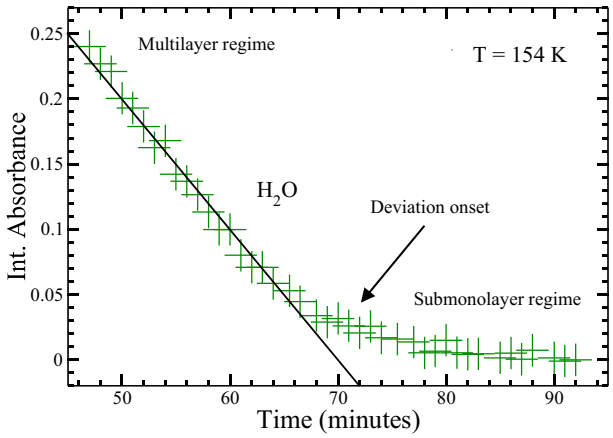

Figure 4.3 Isothermal desorption at 154 K of a thick layer of H_2O ice. The straight line guides the eye to identify the change in the slope of the curve, which corresponds to the transition from zeroth-order to first-order desorption.

layers. The integrated band area oscillates as a function of the layer thickness due to optical interference that is caused by the reflection at both the film-vacuum and film-substrate interfaces. The results presented in this chapter are all in the linear regime, where the modified Lambert-Beer equation still applies. This is verified by depositing pure H_2O ice and checking for non-linearities in the growth rate.

The RAIR difference spectra acquired during an hydrogenation experiment of 35 ML of solid O_2 at 25 K are shown in Fig. 4.2. Both H_2O and H_2O_2 integrated band intensities clearly grow as the H-fluence (H-flux $\times$ time) increases. The inset in Fig. 4.2 also shows the presence of ozone in our RAIR spectra upon H-atom exposure. The $\nu_3(O_3)$ stretching mode peaks at 1038 cm^{-1} in our spectra and corresponds to the band position when solid O_3 is formed and mixed in a polar environment like H_2O:O_2 ices (Cooper et al. 2008). The presence of solid ozone formed upon hydrogenation of O_2 ice provides clear experimental evidence for the incompleteness of the H_2O formation routes considered for decades in astrochemical models. In Chapter 5 these models are extended with a more complete reaction scheme. In this chapter, the focus is on the ice penetration mechanism. Ozone hydrogenation is an efficient formation channel and can contribute to the total water amount in our experiments (Mokrane et al. 2009, Chapter 6). Figure 4.2 shows trace amounts of HO_2 trapped in the ice. The $\nu_3(HO_2)$ band mode peaks at 1140 cm^{-1} in our infrared spectra and corresponds to the band position when HO_2 is trapped in H_2O ices (Cooper et al. 2008). Although the $\nu_3(HO_2)$ mode is weaker than the $\nu_2(HO_2)$ mode, the latter is not visible in our infrared spectra, since it overlaps with strong H_2O_2 bending modes. We did not detect OH radicals here. This may have two reasons; they have either reacted further to form H_2O or H_2O_2 or their infrared features in a H_2O:H_2O_2 ice are too broad to be distinguished from the H_2O and H_2O_2 OH-stretching band modes. In

Chapter 5 we present the spectroscopic detection of OH radicals, which have formed in the ice through surface reactions at an early stage in the reaction scheme, using a different experimental approach.

Two vibrational modes of the newly formed H_2O, peaking at 3430 and 1650 cm^{-1}, are above the noise-level in our RAIR spectra (Fig. 4.2). The broad 3430 cm^{-1} OH-stretching modes (ν_1 and ν_3) of H_2O overlap with the 3250 cm^{-1} stretching modes (ν_1 and ν_5) of H_2O_2. The integrated band area of the OH-stretching modes is at the edge of the linear regime for the experiment carried out at 28 K, where the optimum in the final yield is found. Thus, we have chosen the bending modes, peaking at 1650 cm^{-1} (ν_2) and 1350 cm^{-1} (ν_2, ν_6 and $2\nu_4$), to quantify the column densities of solid H_2O and H_2O_2, respectively. The band modes of D_2O and D_2O_2 ices exhibit systematic peak position shifts of ~400 cm^{-1} towards lower wavenumbers with respect to the H_2O and H_2O_2 band modes. The column densities of the deuterated species are obtained in a similar way as described above.

Since literature values of transmission band strengths cannot be used directly in reflectance measurements, an apparent absorption strength of the various species is calculated from calibration experiments. The determination of this apparent absorption strength is set-up specific. The calibration method is described in Chapter 2. In short, a layer of the selected ice is deposited at a temperature lower than its desorption temperature. The sample is then linearly heated, close to its desorption temperature. Infrared spectra are acquired regularly until the desorption of the ice is complete. The transition from zeroth-order to first-order desorption is assumed to occur at the onset to the submonolayer regime and appears in the desorption curve as a sudden change in slope. Figure 4.3 shows the isothermal desorption of a H_2O ice layer at 154 K. The arrow in the graph indicates the onset of the deviation from constant desorption. The apparent absorption strength in cm^{-1} ML^{-1} is then calculated by relating the observed integrated area to 1 ML in the modified Lambert-Beer equation. The largest uncertainty in the band strengths is due to the uncertainty in the onset of the first-order desorption, which can be affected by the non-wetting property of the gold substrate (hydrophobic surface) in the case of H_2O, for instance. We verified our calibration method by repeating the experiments reported by Fraser et al. (2001) who performed several TPD experiments of H_2O ice deposited on a gold substrate for different ice thicknesses, where the deposited amount of H_2O ice was measured using a quartz crystal microbalance. The desorption order and the position of the desorption peak depend on the deposited amount of H_2O ice. We were able to reproduce their results quantitatively using the H_2O band strength obtained from the isothermal desorption experiment. We estimate the uncertainty of the band strength to be within 50%. In this work, this calibration method is applied to both H_2O and D_2O ice, giving the same band strength value for both.

Pure hydrogen peroxide and deuterium peroxide are experimentally difficult to deposit, because of their chemical instability. In Chapter 3 the apparent absorption strengths are obtained indirectly, assuming the ratio of the integrated band strengths in reflectance between H_2O and H_2O_2 (D_2O and D_2O_2) to be the same as in transmittance H_2O/H_2O_2 = D_2O/D_2O_2 = 0.57 (Gerakines et al. 1995, Loeffler et al. 2006). The H_2O bending mode is very sensitive to the local environment in terms of band shape and width and partially

overlaps with the H_2O_2 bending mode at lower wavenumbers in a mixture. Thus, we obtained the H_2O band strength from calibration experiments, integrating the H_2O bending mode in the range where it does not overlap with the H_2O_2 bending mode, and we determined the band strength ratio in a H_2O_2-rich environment independently. This is done by assuming mass balance in a H_2O_2 hydrogenation experiment between the formed H_2O and reacted H_2O_2 molecules. The H_2O_2 layer is formed on top of the gold substrate by co-depositing H atoms and O_2 molecules with a ratio $H/O_2 = 20$ and heating the substrate to above the O_2 desorption temperature. Details of this experiment are reported in Chapter 5. We find the ratio of the integrated band strengths between H_2O and H_2O_2 (D_2O and D_2O_2) to be 0.31 ± 0.10.

4.2.3 Control experiments

The list of experiments in Table 4.1 contains a number of control experiments. These are performed

1. to verify that new species are formed in the solid phase by surface reactions and not in the gas phase;
2. to check whether the deposition of background H_2O on the substrate is indeed negligible;
3. to confirm that final products are due to surface reactions involving H/D atoms and not H_2/D_2 molecules;
4. to verify that the maximum penetration depth of the atomic hydrogen into the oxygen ice is not larger than the actual O_2 thickness chosen for each experiment;
5. to verify that the gold substrate does not affect the final results.

Point 1 is investigated by the simultaneous deposition of O_2 molecules and D at 60 K. At this temperature O_2 molecules do not stick to the substrate long enough to form an ice layer, while H_2O and H_2O_2 could still freeze-out onto the substrate if they would be formed via gas phase reactions. After 90 minutes of co-deposition no new solid species are detected on the substrate. Point 2 is estimated by exposing an inert $^{15}N_2$ ice layer instead of solid O_2 to H atoms at 15 K for 180 minutes. In this case no newly formed H_2O and H_2O_2 molecules are detected and the background H_2O contamination does not exceed 0.1 ML after 3 hours of H-addition to $^{15}N_2$ ice. Furthermore, we repeated the standard experiment using D atoms instead of H atoms to confirm that solid H_2O is formed in the ice and does not originate from the background. In this case, as shown in Miyauchi et al. (2008), Ioppolo et al. (2008), only solid deuterium peroxide and heavy water are formed. Point 3 is verified by exposing an O_2 layer to H_2 molecules. After 2.5 hours of H_2 addition at 25 K, no new species are formed.

Concerning point 4, a thick O_2 layer (100 ML) is deposited at 15 K and then exposed to an H-atom beam for 5 hours at 28 K. Acharyya et al. (2007) showed that under ultra

high vacuum conditions O_2 thermal desorption starts at ~28 K. Therefore, the O_2 ice thickness can change in time at 28 K upon desorption and experiments at this temperature are not straight-forward. Nevertheless, as in Chapter 3, we find an optimum temperature for the formation of H_2O and H_2O_2 at 28 K. The control experiment performed in this work shows that the O_2 use-up at 28 K, obtained according to reactions (4.7) and (4.2) ($N[O_2] = \frac{1}{2} \times N[H_2O] + N[H_2O_2]$, see § 4.3.4), is ~35 ML. This has to be considered as a lower limit for the maximum penetration depth of the atomic hydrogen into the O_2 ice at 28 K, because of the thermal desorption of the oxygen layer. However, experiments at lower temperatures never reached an O_2 use-up higher than 35 ML. For this reason we decided to use an O_2 ice thickness of 35 ML for most of our experiments and to investigate only temperatures below 28 K, where the O_2 layer does not desorb (see Table 4.1). This thickness is higher than the 15 ML thickness used in Chapter 3 (more details in § 4.3.1). In this work, special care is taken to use low O_2 deposition rates to ensure optimal control of the ice thickness (see Table 4.1). The number of monolayers is calculated assuming a constant O_2 deposition rate. However, during the first minutes of the O_2 deposition the rate is not in a linear regime and, once the deposition valve is closed again, background O_2 molecules still present in the main chamber can still contribute to the total ice thickness. Thus, longer deposition times result in a smaller error in the O_2 ice thickness, because the relative contribution in time of the non-linear deposition rates becomes negligible.

Point 5 is addressed by depositing a thick layer of compact H_2O ice (100 ML) at 120 K and on top a thinner layer of O_2 (15 ML) at 15 K, which is subsequently hydrogenated at 25 K. In this case the O_2 layer will become completely hydrogenated, because the maximum penetration depth of H atoms at 25 K is ~15 ML (see § 4.3.4), but the H atoms cannot reach the gold substrate because of the thick layer of compact H_2O ice (Dulieu et al. 2010, Matar et al. 2008). The result of this experiment is the same as for a similar experiment with the O_2 ice directly deposited on the gold substrate. Thus, the gold substrate is found not to affect the O_2 hydrogenation process within the sensitivity limits of our experiment.

4.3 Results and discussion

In a standard hydrogenation experiment, O_2 ice is deposited at 15 K with a thickness of 35 ML. After deposition the ice is slowly heated to the required temperature, with a rate of 1 K min^{-1}, and subsequently exposed to an H-atom flux of ~2.5×10^{13} atoms cm^{-2} s^{-1} for several hours.

4.3.1 Temperature dependence

Experiments are performed for different temperatures in the range between 15 and 27 K. The aim of this section is to study the effect of the ice temperature on the formation rate of H_2O and H_2O_2 and final yield, investigating in more detail than in Chapter 3 temperatures above 20 K, where an optimum in the final yield was found. Figure 4.4 plots the column

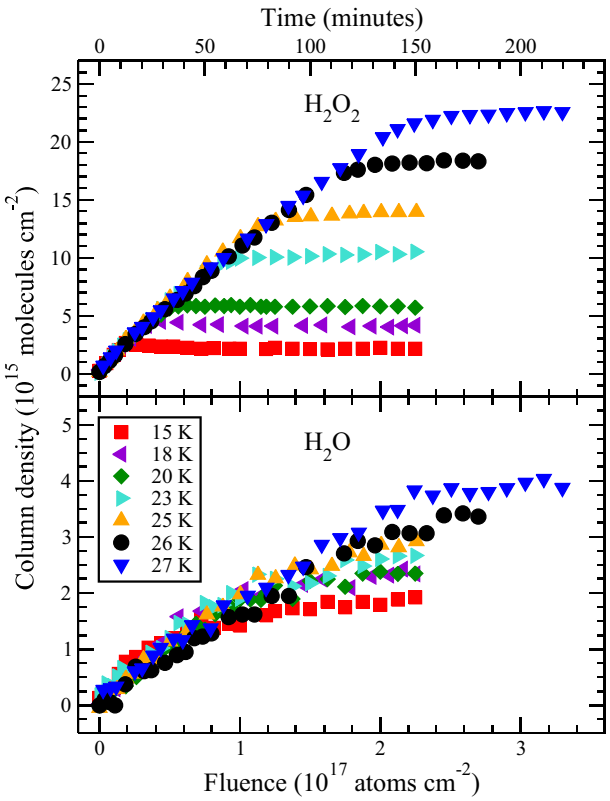

Figure 4.4 Temperature dependence of the H_2O_2 (*top*) and H_2O (*bottom*) column densities as a function of the H-atom fluence and time of H-atom exposure.

densities of H_2O and H_2O_2 as a function of the H-fluence for all the considered substrate temperatures. In each experiment, the final H_2O_2 yield is higher than the H_2O yield resulting in smaller relative errors for the H_2O_2 data. For all temperatures, the solid H_2O_2 column density shows the same initial linear increase followed by a relatively sharp transition to a steady state regime, with the final yield increasing with temperature. The solid H_2O column densities exhibit a similar behavior, but the transition is not as sharp as in the H_2O_2 case and the temperature dependence of the final yield is not as pronounced.

The experimental results presented in this section reproduce those discussed in Chapter 3 for temperatures below 23 K, once results presented in Chapter 3 are scaled with the H_2O_2 band strength value used in this work. For temperatures above 23 K the H_2O and H_2O_2 final yield is found to be higher in this work than in Chapter 3, while the formation rate is the same in both studies for all the investigated temperatures. As discussed above, a different O_2 deposition rate at 15 K in the two studies (1.5 ML min^{-1} Chapter 3 vs. 0.7 ML min^{-1} this chapter) caused an initial different O_2 ice thickness (15 ML in Chapter 3 according to the O_2 use-up vs. 35 ML this chapter). The different O_2 ice thicknesses may explain the discrepancy between the two studies in the H_2O and H_2O_2 final yield for temperatures above 23 K, where the hydrogen can penetrate deeper into the ice than 15 ML. Details are reported in § 4.2.3 and § 4.3.4.

The initial constant formation rate and the high final yield of tens of monolayers (see Fig. 4.4) indicate that the hydrogenation reaction of solid O_2 is a bulk process that does not involve the surface of the ice only. H atoms diffuse into the O_2 ice with a penetration depth which is temperature dependent. This is different from the case of CO hydrogenation, in which only ~4 ML are involved in the reactions and minimal amounts of final products are detected in experiments at temperatures higher than 16 K, due to H-atom desorption at high temperatures (Watanabe et al. 2004, Fuchs et al. 2009). In the case of O_2, however, H atoms penetrate deeper into the ice at high temperatures (>20 K). Moreover, the constant formation rate shows that even at high temperatures the desorption of H atoms from the ice is a negligible process. Thus, H atoms can penetrate deep and stay into the oxygen ice long enough to react with O_2.

The temperature dependence of the penetration depth can have several origins. It is possible that for higher temperatures the O_2 ice is less rigid and the mobility of the O_2 atoms facilitates the penetration into the ice by moving to the side. However, more thermal vibration of O_2 molecules leads to larger effective radii, which may also hinder the H atoms while passing. We would therefore expect the penetration depth to have an optimum temperature (as in the case of CO ice hydrogenation around 15 K) when there is high H-atom mobility but not too much thermal vibration of O_2 molecules, and this has not been found. This is therefore not likely the dominant mechanism responsible for the temperature dependence of the H-atom penetration. A second possibility could be that at higher temperature the oxygen layer slowly converts from amorphous to crystalline which is more effective to penetrate. A third scenario is that the hydrogen atoms do not really penetrate the ice, but that mobile oxygen molecules keep replenishing the top layers. A final possible scenario involves the ratio between the rate of the barrierless reaction between hydrogen and solid O_2, which is temperature independent, and the rate of the thermally activated process of hydrogen diffusion into the ice, which increases with

temperature. In this scenario, at each O_2 layer that the H atom passes, it has a probability to react with the O_2 ice or to penetrate deeper into the ice. At low temperature, reaction is favored; at high temperature, penetration. Thus, for this explanation the penetration length of an individual atom is a stochastic process and the average length depends on the temperature of the ice. In the following sections we will discuss in more detail the latter three scenarios proposed here: restructuring of the O_2 ice, replenishing of the top layers and competition between reaction and diffusion. We will experimentally show that the competition between reaction and diffusion is the most likely scenario.

4.3.2 Structural effect

The yield of the final products in the experiments at high temperatures (>20 K) show that hydrogen atoms can penetrate the ice over several monolayers. One possible explanation for the efficient diffusion of H atoms into the ice for higher temperatures is, as mentioned before, a higher crystalline fraction in the structure of the ice at higher temperature. To verify this hypothesis an O_2 layer deposited at 15 K is annealed at 25 K before H-atom addition at 15 K. This experiment is meant to investigate the effects of possible irreversible structural changes, which could take place at temperatures slightly below the desorption temperature of O_2 (Kreutz et al. 2004). Infrared spectroscopy does not allow us to investigate different phases of solid O_2. Nevertheless, if the change in the ice structure would play an important role in the O_2 hydrogenation experiments, one would expect to obtain a higher final yield of the products than in a standard O_2 hydrogenation experiment at 15 K. However, the H_2O and H_2O_2 formation rates and final yield in the annealing and in the standard experiment at 15 K are all comparable within the experimental uncertainties (see Fig. 4.5).

It should be noted that if a structural change from amorphous to crystalline in the ice is present at high temperatures a different incident angle of the H-atom beam could still affect the rate reaction and final yield of the end products. We compared results from a 25 K experiment of H-atom addition with an incident angle of 45° to those obtained from an experiment, where the H-atom beam is normal to the substrate surface. In both cases the geometry of the infrared optics is kept the same, since the H-atom beam was stopped and the sample turned back to 90° to the the H-atom beam each time an infrared spectrum was acquired. The infrared beam is in both cases wider than the projection of the H-atom beam on the substrate. Figure 4.6 shows that formation rate and final yield of the products are the same in both cases. Thus, the higher penetration depth of the H atoms into the ice at high temperatures is most likely due to one of the two remaining scenarios: replenishing or reaction vs. diffusion.

As a further extension, Fig. 4.5 shows also an experiment performed at 15 K in which H-atom addition is interrupted upon saturation of H_2O_2 (*triangle*). This experiment is performed to confirm that the decrease in H_2O_2 after saturation is due to reaction and not to desorption. We will come back to this point later.

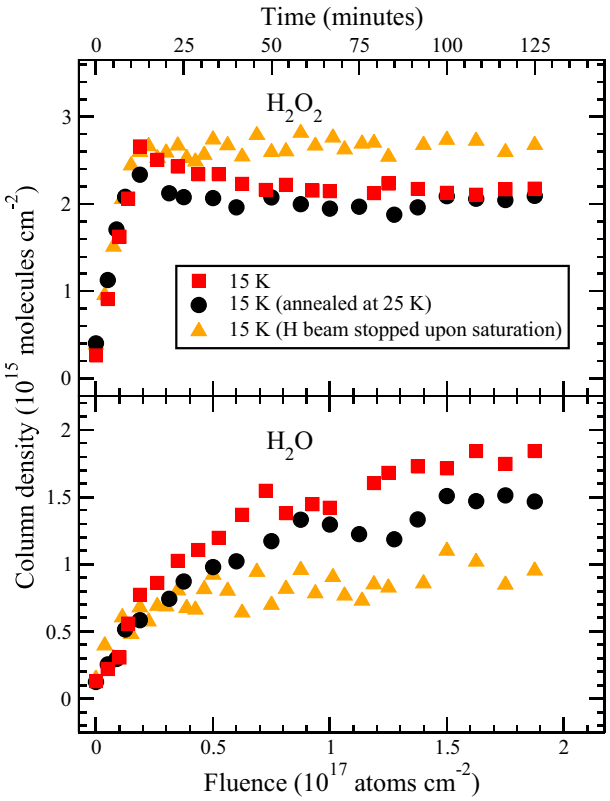

Figure 4.5 The H_2O_2 (*top*) and H_2O (*bottom*) column densities as a function of the H-atom fluence and time of H-atom exposure for a standard experiment performed at 15 K (*square*) compared to an experiment in which an O_2 layer deposited at 15 K is annealed at 25 K before H-atom addition (*circle*). Also shown is an experiment in which the H-atom addition is stopped upon H_2O_2 column density saturation (*triangle*).

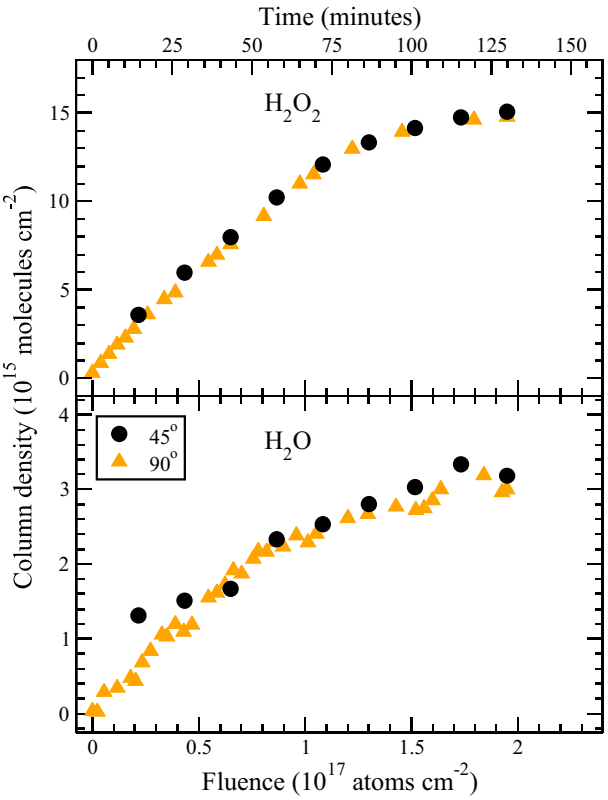

Figure 4.6 H_2O_2 (*top*) and H_2O (*bottom*) column densities as a function of the H-atom fluence and time of H-atom exposure for an experiment performed at 25 K, in which the H-atom beam has an incident angle to the O_2 ice of 45° (*circle*), compared to a similar experiment, in which the H-atom beam is normal to the substrate surface (*triangle*).

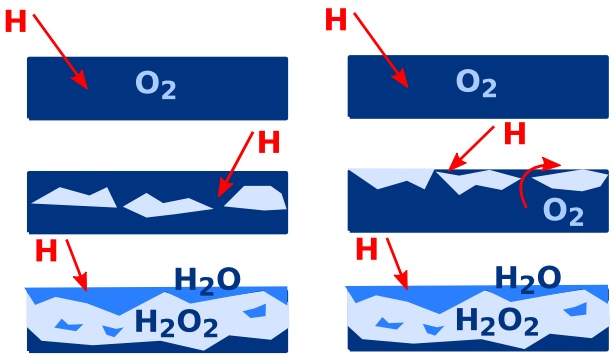

Figure 4.7 Schematic representation of two penetration scenarios: (*left*) competition between reaction and diffusion (*mainly bottom-up*) and (*right*) replenishing of the top layers by O_2 mobility (*top-down*).

4.3.3 Penetration mechanism

In the previous sections we gave experimental evidence for the importance of the hydrogen penetration depth into O_2 ice ruling out two possible mechanisms. The purpose of this section is to investigate whether the high H-atom penetration depth is due to the competition between reaction and diffusion or replenishing of the top layers by mobile O_2 molecules. The two scenarios are schematically depicted in Fig. 4.7. In the first case, O_2 is hydrogenated mainly bottom to top, in the latter top to bottom.

Using thick O_2 ices (see Table 4.1), we performed the experiments shown in Fig. 4.8. In the first experiment we added H atoms to the O_2 ice at 15 K until the column density of the newly formed species was saturated (O_2 use-up = 2.5 ML). After interrupting the hydrogenation we heated the ice to 25 K and added H atoms until a new saturation level was found (total O_2 use-up = 4 ML). We repeated the same experiment hydrogenating an identical ice at a temperature of 25 K, until saturation (O_2 use-up = 13 ML), then we cooled it to 15 K and hydrogenated it for 70 minutes (total O_2 use-up = 13 ML). In the third experiment we hydrogenated another O_2 ice at 25 K, interrupting the H-atom addition before saturation (O_2 use-up = 5.5 ML). Then, we cooled it to 15 K and hydrogenated it for 109 minutes (total O_2 use-up = 6.5 ML).

Figure 4.8 shows that the results from these three experiments differ. The final yield of the newly formed species and the final O_2 use-up are not the same in the first two experiments. The O_2 use-up is ~4 ML for an O_2 ice hydrogenated at 15 K and then at 25 K, while it is ~13 ML for an O_2 ice directly hydrogenated at 25 K. In the competition scenario, the H atoms have to penetrate 2 ML of O_2 molecules already converted into H_2O and H_2O_2, if we hydrogenate an O_2 ice at 25 K, which was previously hydrogenated at 15 K. In this case the final hydrogen penetration depth into the ice is just 4 ML and not 13 ML, because the penetration depth of the H atoms into solid H_2O and H_2O_2 is lower than into pure O_2 ice. This result leads us to hypothesize that the hydrogenation follows

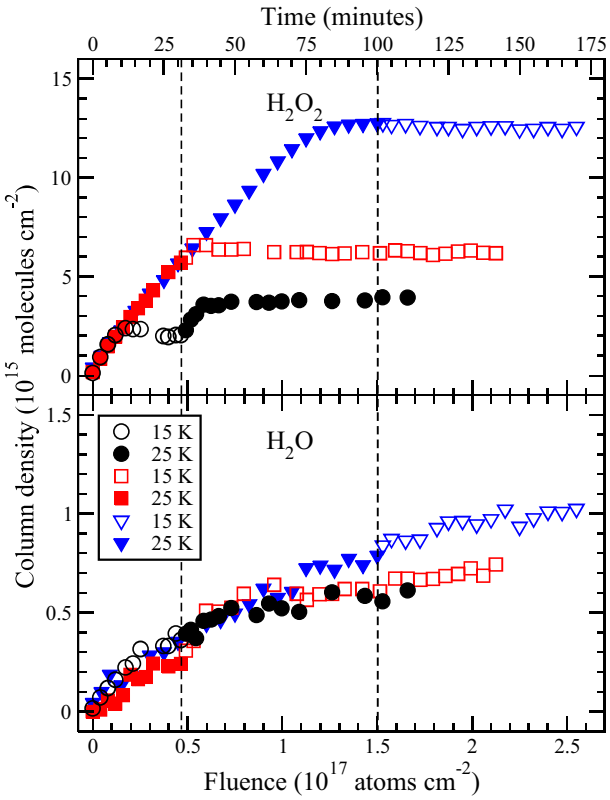

Figure 4.8 The H_2O_2 (*top*) and H_2O (*bottom*) column densities as a function of the H-atom fluence and time of H-atom exposure for an experiment in which H atoms are added to the O_2 ice at 15 K (*open symbols*) until saturation of the column densities and, then, at 25 K (*closed symbols*) until a new saturation level was found (*circle*); the same experiment, inverting the order of the temperatures for the H-atom addition (*triangle*); an experiment in which the hydrogenation of the O_2 ice at 25 K is stopped before saturation and, then, continued at 15 K (*square*).

a distribution that starts mainly from the bottom layers of the ice to the top. If instead the replenishing of the top layers due to a higher O_2 molecules mobility in the ice for higher temperatures would play an important role in the O_2 hydrogenation, we would expect to get the same final yield for both experiments. This is not the case.

In the third experiment we interrupted the hydrogenation process when 5.5 ML of the ice were converted into H_2O and H_2O_2 at 25 K. If the hydrogenation would start straight from the bottom layers to the top, the top layers of the ice would have not yet been hydrogenated and we would expect to hydrogenate up to an extra 2.5 ML of ice at 15 K in the second part of the experiment, whereas we observed the hydrogenation of only 1 ML of ice. The final O_2 use-up is probably not reached because the H atoms are blocked by some of the H_2O and H_2O_2 molecules, which are earlier formed in the upper layer of the ice according to the competition scenario, which involves mainly the bottom layers and partially the top layers of the O_2 ice in the early stage of the hydrogenation.

Thus, all experiments presented so far are in accordance with the following scenario: first, the H atoms penetrate into the ice without desorbing. The penetration depth is determined by a temperature dependent competition between reaction with O_2 molecules and further diffusion into the ice. In this way, the ice is hydrogenated following a distribution that involves mainly the bottom layers and partially the top layers at the beginning. Subsequently, the penetration depth of atoms that enter the ice in a later stage is determined by the competition mechanism until they reach species other than O_2.

4.3.4 Thickness dependence

Different thicknesses are studied in the range between 1 and 35 ML. The O_2 ice is deposited at 15 K with a rate of ~0.3 ML min^{-1} to better control the ice thickness during deposition and then heated to 25 K. The ice layer is subsequently exposed to H atoms, in most of the cases, for 150 minutes with a total H-atom fluence of 2.2×10^{17} atoms cm^{-2}. Figure 4.9 plots the column density of H_2O_2 and H_2O versus the fluence of impinging H atoms on the solid O_2 layer for different thicknesses.

Again, the initial formation rate of H_2O and H_2O_2 is constant and thickness independent, while the final yield is thickness dependent and is affected by the penetration depth of the H atoms into the ice. The O_2 ice is indeed completely converted into H_2O and H_2O_2 for layers thinner than the maximal penetration depth of the H atoms into the ice at 25 K (low oxygen coverage). For layers thicker than the maximal penetration depth of the H atoms into the ice, some O_2 is not hydrogenated (high oxygen coverage). Figure 4.10 shows the final yield for H_2O and H_2O_2 formation as well as the O_2 use-up as a function of the initial O_2 thickness. The O_2 use-up is estimated by adding half of the newly formed H_2O column density to the H_2O_2 column density ($N[O_2] = \frac{1}{2} \times N[H_2O] + N[H_2O_2]$), according to reactions (4.7) and (4.2), where, from each O_2 molecule, two H_2O molecules can be formed. Figure 4.10 shows that the maximal penetration depth at 25 K is reached in the high oxygen coverage regime (>15 ML) and is ~16 ML.

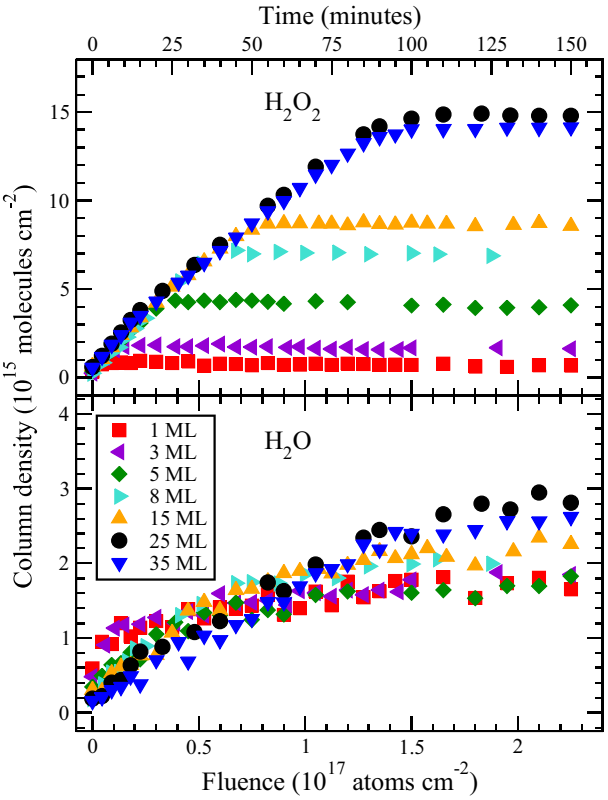

Figure 4.9 Thickness dependence on the H_2O_2 (*top*) and H_2O (*bottom*) column densities as a function of the H-atom fluence and time of H-atom exposure at 25 K.

The O_2 use-up ($N[O_2]$) is fitted with the following function:

$$N[O_2] = \left((a\vartheta)^{-2} + (b)^{-2}\right)^{-\frac{1}{2}} \tag{4.9}$$

where a and b are fitting parameters and ϑ is the initial O_2 thickness. Equation 4.9 is a combination of two linear functions describing the O_2 use-up in the two extreme regimes. For low coverage, the yield is expected to be equal to the coverage $N[O_2] = a\vartheta$, with $a = 1$. At high coverage, the yield will be equal to the maximum penetration depth, b. The fit to the data gives $a = 1$, as we expected, and $b = 16$ ML. The transition between the two linear regimes is not sharp. This can be explained by considering that the penetration length of the H atoms is not one absolute value, but covers a distribution with an average value of 16 ML at 25 K. In the case of a 16 ML thick O_2 ice, the high end of the distribution will be missing, resulting in a lower average value. This is again in agreement with the competition scenario. Results from the control experiment of 15 ML of O_2 deposited on top of a compact H_2O layer, plotted in Fig. 4.10, confirm the scenario described above. In

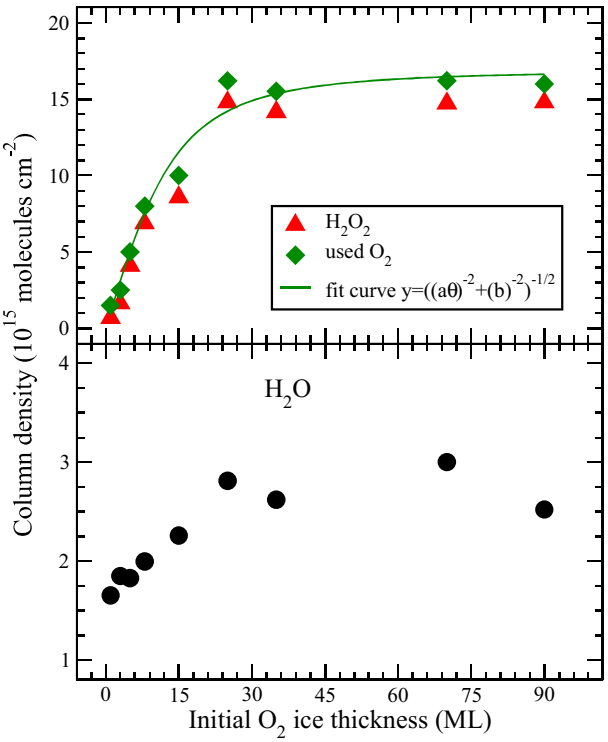

Figure 4.10 Final yields for H_2O_2 (*top*, *triangle*) and H_2O (*bottom*, *circle*) and O_2 use-up (*top*, *diamond*) as a function of the initial O_2 thickness at 25 K. The line is the fit curve to the O_2 use-up data. Data from the control experiment of 15 ML of O_2 deposited on top of a compact H_2O ice are also plotted and included in the fit.

this case less than 15 ML of O_2 are hydrogenated. Correlating the O_2 use-up expressed in monolayers to our O_2 deposition flow in Langmuir, we have an independent estimate of the O_2 ice thickness for all our experiments, which leads to a correspondence of 3 L to 1 ML.

For oxygen films thinner than 5 ML, more H_2O is formed initially and almost all H_2O_2 formed at low fluence is later converted into H_2O. This can be explained by the fact that H atoms are more likely to find H_2O_2 to react with in thin O_2 layers than in thick O_2 layers for the same absolute amount of H_2O_2. This confirms that H_2O formation can proceed with H_2O_2 as a precursor (reaction (4.7)). Figure 4.5 indeed shows that the decrease in H_2O_2 is due to reaction. The figure clearly shows that reaction (4.7) is stopped and H_2O_2 is not converted to form H_2O. In Chapter 5 we will discuss in more detail this reaction channel.

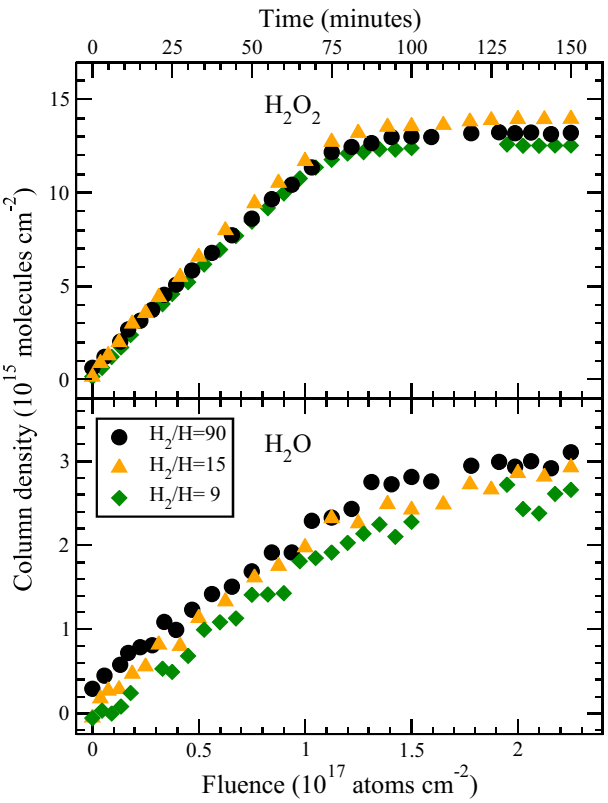

Figure 4.11 The H_2O_2 (*top*) and H_2O (*bottom*) column densities as a function of the H-atom fluence and time of H-atom exposure for different H_2/H ratios at 25 K.

4.3.5 H_2 dependence

Reaction (4.3) could play a role in the solid phase, even though it has a barrier in the gas phase. By controlling the H_2 flow into the thermal cracking source and the filament temperature, different hydrogen fluxes and different H_2/H ratios can be realized. The role of H_2 in surface reactions is investigated comparing the results of three similar experiments at 25 K in which the same H-atom flux, but different H_2/H ratios, are used. The details about these experiments are reported in Table 4.1. From flux measurements (see Appendix A) we estimate the H_2/H ratio to vary between 9 and 90. If reaction (4.3) is important and if a significant amount of OH radicals is present in the ice, the H_2O abundance should be higher in the case of more H_2. Figure 4.11 shows that the formation rate and the final column densities of both H_2O and H_2O_2 are the same in all cases within the experimental errors. This indicates that H_2 molecules, formed through surface reactions in the ice or along the quartz pipe or originating from the not-fully dissociated

H-beam, do not have any measurable effect on the O_2 reaction channel and consequently that reaction (4.3) is not an important route for H_2O formation in our experiments.

4.4 Conclusion

An extensive complementary study of Chapter 3 is presented under ultra high vacuum conditions at temperatures between 15 and 28 K. RAIR spectra are used to analyze the results and calibration experiments are performed to measure atomic fluxes and band strengths of the newly formed species. From this quantitative study we draw the following conclusions:

1. The initial constant H_2O and H_2O_2 formation rate is temperature and thickness independent. The final yield is temperature and thickness dependent and is probably governed by the competition between the reaction of atomic hydrogen with the solid O_2 and the hydrogen diffusion into the ice, which is temperature and thickness dependent.

2. The penetration depth of the H atoms into the ice is affected by the competition between reaction and diffusion and increases with temperature. H atoms penetrate into the bulk of the ice with a penetration depth (up to ~35 ML at 28 K), that is temperature dependent. Once an H atom is trapped into the ice, it diffuses efficiently and finds an oxygen molecule to react with.

3. The ice is hydrogenated initially mainly bottom-up and partially from the top layers. The penetration length of the H atoms covers a distribution of values with an average value which corresponds to the maximum penetration depth measured, which is temperature dependent. Experimental evidence shows that the model used in Chapter 3 and described in the introduction of the present chapter to fit the experimental data not only reproduces the laboratory data, but also has physicochemical meaning; it explains the behavior of the H-atom diffusion into the O_2 ice for the conditions investigated here. This also corrects statements made in Oba et al. (2009).

4. H_2O and H_2O_2 formation via the molecular oxygen channel proposed by Tielens & Hagen (1982) is experimentally proven to be efficient under laboratory conditions. Nevertheless, other reactions should be considered in the reaction route as well. The presence of solid ozone formed in the ice, under the experimental conditions described here, gives a clear experimental evidence for the incompleteness of the H_2O formation routes considered for decades in astrochemical models (more will be presented in Chapter 5).

5. H_2 molecules do not take a relevant part in the reaction scheme at a detectable level, for the temperature range investigated.

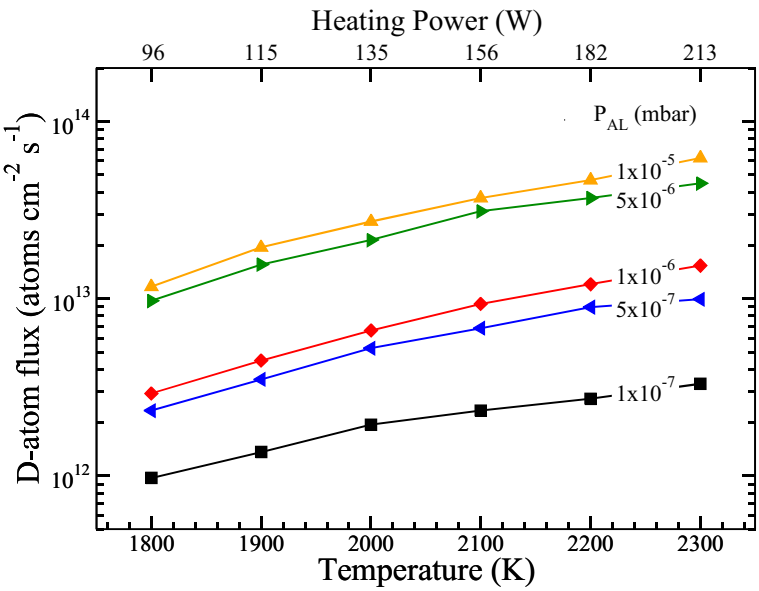

Figure 4.12 The D-atom fluxes at the substrate site plotted versus different parameter settings: temperature of the tungsten filament, heating power and atomic line pressure. The lines connecting data points guide the eye and are not best-fits.

Appendix A: Absolute atomic flux determination

Absolute atomic fluxes are measured in the main chamber, following the procedure described in Hidaka et al. (2007). Since the sensitivity of the standard 1−200 amu QMS does not allow an accurate measurement at mass 1, we decided to measure D-atom fluxes. For this the substrate was removed and the inlet of the QMS was placed at the center of the chamber in sight of the atomic line, exactly at the position where the ice is hydrogenated. Once the source was turned on, the increase in intensity of the D atoms was monitored with the QMS with a Faraday cup. The QMS measurements do not directly give the D-atom flux values, but the increase in intensity of the QMS signal, ΔQ_{D}, is proportional to the increase in pressure in the main chamber, ΔP_{D}:

$$\Delta P_{\mathrm{D}} = a \Delta Q_{\mathrm{D}} \tag{4.10}$$

We measured the proportionality factor a, which is independent of the gas species, introducing D_2 molecules instead of D atoms in the main chamber, since the D-atom beam contains a significant amount of D_2 molecules and an exact measurement of ΔP_{D} is not straight-forward from pressure gauges. A constant factor a was determined for all main chamber and atomic line pressures that were used during the experiments. The

absolute D-atom flux is then obtained from the following expression:

$$f_{\mathrm{D}} = \frac{c_{\mathrm{D}} \Delta P_{\mathrm{D}} \langle v \rangle}{4 k_{\mathrm{B}} T} = \frac{c_{\mathrm{D}} a \Delta Q_{\mathrm{D}} \langle v \rangle}{4 k_{\mathrm{B}} T} \tag{4.11}$$

where c_{D} is the calibration factor for the pressure gauge for D atoms taken from the manual, $\langle v \rangle$ is the thermal velocity of the D atoms at 300 K, k_{B} is the Boltzmann constant, and T is the D-atom temperature. By changing the filament temperature and/or the D_2 inlet flow, the D-atom flux can be varied between 10^{12}–10^{14} atoms cm^{-2} s^{-1}. Figure 4.12 shows the D-atom flux values measured at the substrate site for different parameter settings.

The H-atom flux value used in all the experiments presented here, is determined by comparing the H_2O_2 and D_2O_2 formation rate, which is flux dependent, in two identical 25 K experiments with a filament temperature of 2200 K and an atomic chamber pressure of 1×10^{-6} mbar. The resulting H-atom flux at the surface site is a factor of two higher than the D-atom flux measured. This can be explained by the difference in mass between hydrogen and deuterium, which affects the atomic thermal velocity, and the cracking efficiency in the source. The final H-atom flux value of 2.5×10^{13} atoms cm^{-2} s^{-1} confirms the value previously estimated and used in Chapter 2 and 3. The relative error for D-atom fluxes is within 10%, for H-atom fluxes within 50%. The absolute error is within 50%.